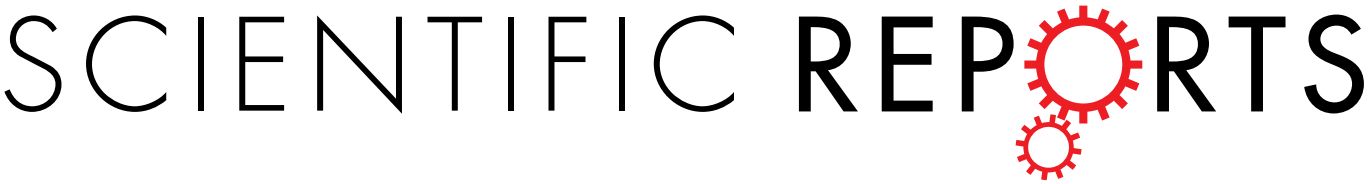

OPEN

Magnetic moment evolution and spin freezing in doped $BaFe_2As_2$

Jonathan Pelliciari[1,7], Yaobo Huang[1,2], Kenji Ishii[3], Chenglin Zhang[4], Pengcheng Dai[4], Gen Fu Chen[2], Lingyi Xing[2], Xiancheng Wang[2], Changqing Jin[2,5], Hong Ding[2], Philipp Werner[6] & Thorsten Schmitt[1]

Received: 23 September 2016
Accepted: 27 June 2017
Published online: 14 August 2017

Fe-K_β X-ray emission spectroscopy measurements reveal an asymmetric doping dependence of the magnetic moments μ_{bare} in electron- and hole-doped $BaFe_2As_2$. At low temperature, μ_{bare} is nearly constant in hole-doped samples, whereas it decreases upon electron doping. Increasing temperature substantially enhances μ_{bare} in the hole-doped region, which is naturally explained by the theoretically predicted crossover into a spin-frozen state. Our measurements demonstrate the importance of Hund's-coupling and electronic correlations, especially for hole-doped $BaFe_2As_2$, and the inadequacy of a fully localized or fully itinerant description of the 122 family of Fe pnictides.

Soon after the discovery of high temperature superconductivity in Fe pnictides[1], antiferromagnetic ordering in the form of a spin-density wave has been observed in the parent compounds[2,3]. The nature of this antiferromagnetism has been highly debated, as demonstrated by the use of antipodal theoretical descriptions, namely, the itinerant and the localized one[2–7]. In the former, magnetism arises from Fermi surface nesting in a similar way to metallic Cr[8], where this phenomenon leads to spin-density wave ordering caused by a diverging susceptibility at the nesting wavevector. In Fe pnictides, the discovery, by means of angle resolved photoemission spectroscopy, of cylindrical hole and electron pockets satisfying these nesting conditions supported such a picture, together with the metallic ground state, and apparently low electronic correlations[2,3,9–11]. However, this weak-coupling scenario could not explain some characteristic properties of Fe pnictides, such as the presence of magnetic moments (μ) at high temperature, outside the antiferromagnetic phase, and the persistence of spin excitations in non-magnetically ordered phases[6,12–20]. These two aspects are more consistently explained in a strong-coupling picture, where strong electronic correlations localize the spins as in Mott-Hubbard-like scenarios[21–23]. However, the metallicity and low μ of Fe pnictides conflict with such an extreme strong coupling description.

A formalism which can handle both the itinerant and localized nature of electrons is the dynamical mean field theory (DMFT)[24]. Thanks to fairly recent methodological advances[25,26], this formalism can efficiently handle the strongly-correlated metal regime of multi-orbital Hubbard models, such as those relevant for the description of Fe pnictides. An important theoretical prediction from DMFT studies[27–30] is the phenomenon of *spin-freezing* (SF). In systems with strong Hund's-coupling, long-lived magnetic moments appear in the metal phase, if the filling and interaction strength place the system in the vicinity of the half-filled Mott insulator. The magnetic moment has been measured in $BaFe_2As_2$[2,3,5,6,15], but scant spectroscopic information is available on the temperature and doping effects on μ. Moreover, the electron itinerancy, i.e. the dynamics of the electrons, leads to quantum fluctuations, which by time-averaging mask the value of μ observed by slow probes (i.e. neutron diffraction, NMR, and muon relaxation measurements[7,20,31–42]), making it difficult to extract the "bare" value of μ. Fast spectroscopies, probing at the timescale of the electron dynamics (on the order of femtoseconds), are therefore essential to obtain snapshots of the value of μ. This is achieved by the use of techniques such as photoelectron, X-ray absorption, and X-Ray emission spectroscopy[14–20,43], which indeed produce higher values of μ compared to their slower counterparts. Additionally, as explained in refs 17, 44, it is possible to distinguish different aspects of μ, the bare μ ($\mu_{bare} \propto \langle S_i \rangle$) connected to quantum fluctuations and the correlated μ $\left(\mu_{corr} \propto \sqrt{\langle S_i \cdot S_{i+1} \rangle}\right)$,

[1]Research Department Synchrotron Radiation and Nanotechnology, Paul Scherrer Institut, CH-5232, Villigen PSI, Switzerland. [2]Beijing National Lab for Condensed Matter Physics, Institute of Physics, Chinese Academy of Sciences, Beijing, 100190, China. [3]Synchrotron Radiation Research Center, National Institutes for Quantum and Radiological Science and Technology, Sayo, Hyogo, 679-5148, Japan. [4]Department of Physics and Astronomy, Rice University, Houston, Texas, 77005, USA. [5]Collaborative Innovation Center for Quantum Matters, Beijing, China. [6]Department of Physics, University of Fribourg, Chemin du Musée 3, CH-1700, Fribourg, Switzerland. [7]Present address: Department of Physics, Massachusetts Institute of Technology, Cambridge, MA, 02139, USA. Correspondence and requests for materials should be addressed to J.P. (email: jonathan.pelliciari@gmail.com) or T.S. (email: thorsten.schmitt@psi.ch)

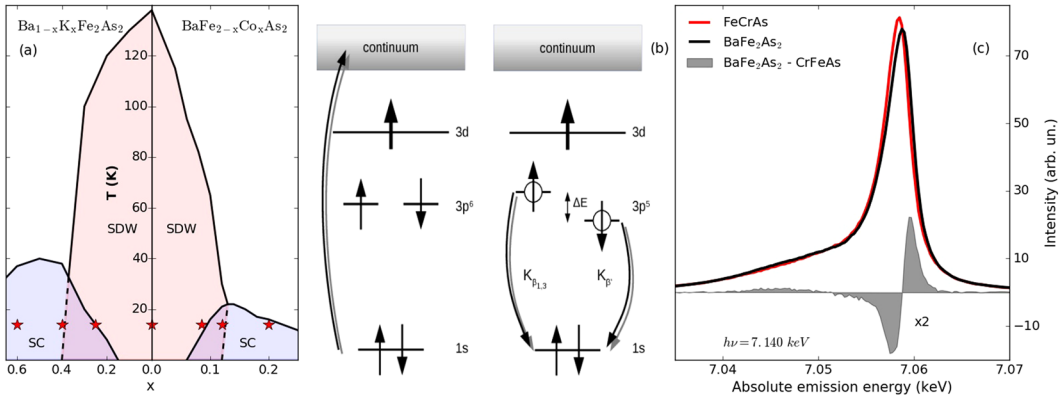

Figure 1. (**a**) Phase diagram of $Ba_{1-x}K_xFe_2As_2$ and $Ba_{1-x}K_xFe_2As_2$. The red stars depict the doping levels measured. (**b**) Sketch of the XES process. (**c**) Exemplary Fe-K_β XES for FeCrAs and $BaFe_2As_2$ at 15 K. The former is taken as a reference and the difference spectrum is obtained (see main text) and depicted as gray shadowed curve.

which is indicative of dressed quasiparticles (spin excitations). These physical entities represent different aspects of magnetism, have different characteristic time and energy scales, and are probed by different experimental techniques[20]. μ_{bare} is detected by local probes such as photoelectron, X-ray absorption, and X-Ray emission spectroscopy[14,15,19,20,45–47], whereas μ_{corr} is measured by employing inelastic spectroscopies, such as inelastic neutron scattering[6,48,49] and resonant inelastic X-ray scattering[12,13,50,51].

In this paper, we present Fe-K_β X-ray emission spectroscopy (XES) measurements of μ_{bare} in electron- ($BaFe_{2-x}Co_xAs_2$) and hole-doped ($Ba_{1-x}K_xFe_2As_2$) Fe pnictides. As outlined in Fig. 1(a) by the stars, our study covers a large range of the phase diagram, from underdoped to overdoped for both electron and hole doping. As we will show, at 15 K, in hole-doped compounds, μ_{bare} exhibits a weak doping dependence, keeping a value around 1.3 μ_B, typical of the parent compound whereas in electron-doped $BaFe_2As_2$, a decrease is observed, with μ_{bare} being gradually quenched to 1.1 μ_B (or 85% of the values of the parent) for the most overdoped sample. While increasing the temperature to 300 K enhances μ_{bare} in all samples, this effect is more pronounced in hole-doped samples than in electron-doped ones. This shows the inadequacy of a fully itinerant approach to explain the formation of local moments and underlines the importance of Hund's-coupling and electronic correlations in Fe pnictides.

A much more consistent explanation of the doping and temperature evolution of μ_{bare} can be given, with the aid of DMFT calculations, in terms of SF. In $BaFe_2As_2$, the nominal d^6 occupation and intermediate strength of the electronic correlations imply that the undoped compound is close to the SF crossover regime[30]. Upon hole doping, as the d-filling approaches $n_d = 5$ (half-filling), the effect of the Hund's-coupling increases, frozen moments appear, and the resulting scattering leads to short quasi-particle life-times and an ill-defined bandstructure. Electron doping, on the other hand, results in a more conventional Fermi-liquid metal, with a well-defined bandstructure and Fermi surface. The electronic screening of μ, by a multi-channel Kondo effect[52], leads to an unusual temperature dependence: μ increases with increasing temperature due to a weaker screening effect. Frozen moments with very low Kondo screening temperature appear in the strongly hole-doped region, while electron doping nudges the system towards a more conventional Fermi liquid state with a reduced μ. In the spin-freezing crossover regime, the Kondo screening temperature varies strongly with doping and we hence expect a large temperature variation of the local moment.

Results and Discussions

XES has been established as an extremely sensitive technique in the detection of μ_{bare}[14–16,43,45–47,51,53–55]. In this spectroscopy a core-electron from the Fe 1s core-shell is excited into the continuum by a photon (in our case $h\nu = 7.140$ keV), the core-hole is then filled up by a Fe 3 p electron together with the emission of a photon ($h\nu = 7.040$–7.065 keV), as shown by the scheme in Fig. 1(b). The final state, being Fe 3 p^5, has a wavefunction partly overlapping with the Fe 3 d orbitals, which is consequently affected by the spin polarization of the valence band[56,57]. This gives rise to a main emission line (composed of $K_{\beta 1}$ and $K_{\beta 3}$) and a satellite peak ($K_{\beta'}$) as shown in Fig. 1(b). The relative intensity of these peaks directly depends on the Fe 3 d net spin[14–16,43,45–47,51,53–55], and employing a calibration procedure, a quantitative determination of μ_{bare} is possible. This method probes the fs timescale[20] allowing the measurement of $\mu_{bare} \propto \langle S_i \rangle$ and minimizing the problem of electron dynamics decreasing the measured value of the moment. By probing the femtosecond fluctuations of the magnetic moment, this technique gives access to the ultrafast dynamics of the local magnetism. However, it is important to differentiate it from time resolved and pump-probe experiments, which can tune and control the probed time scale.

In Fig. 1(c), we show XES spectra obtained from FeCrAs and $BaFe_2As_2$. The former is employed as a standard material due to $\mu_{bare} = 0$ on the Fe sublattice, together with a similar Fe coordination to the samples investigated[58,59]. $BaFe_2As_2$ has been employed as the high μ_{bare} standard, setting it to a value of 1.3 μ_B taken from ref. 15. To determine μ_{bare}, we employed the integrated absolute difference (IAD) method described in ref. 54. The areas of the spectra are normalized and the difference to the reference spectrum of FeCrAs is calculated. The integration of this difference gives the IAD, which is proportional to μ_{bare}. To calibrate the absolute energy, we aligned in an

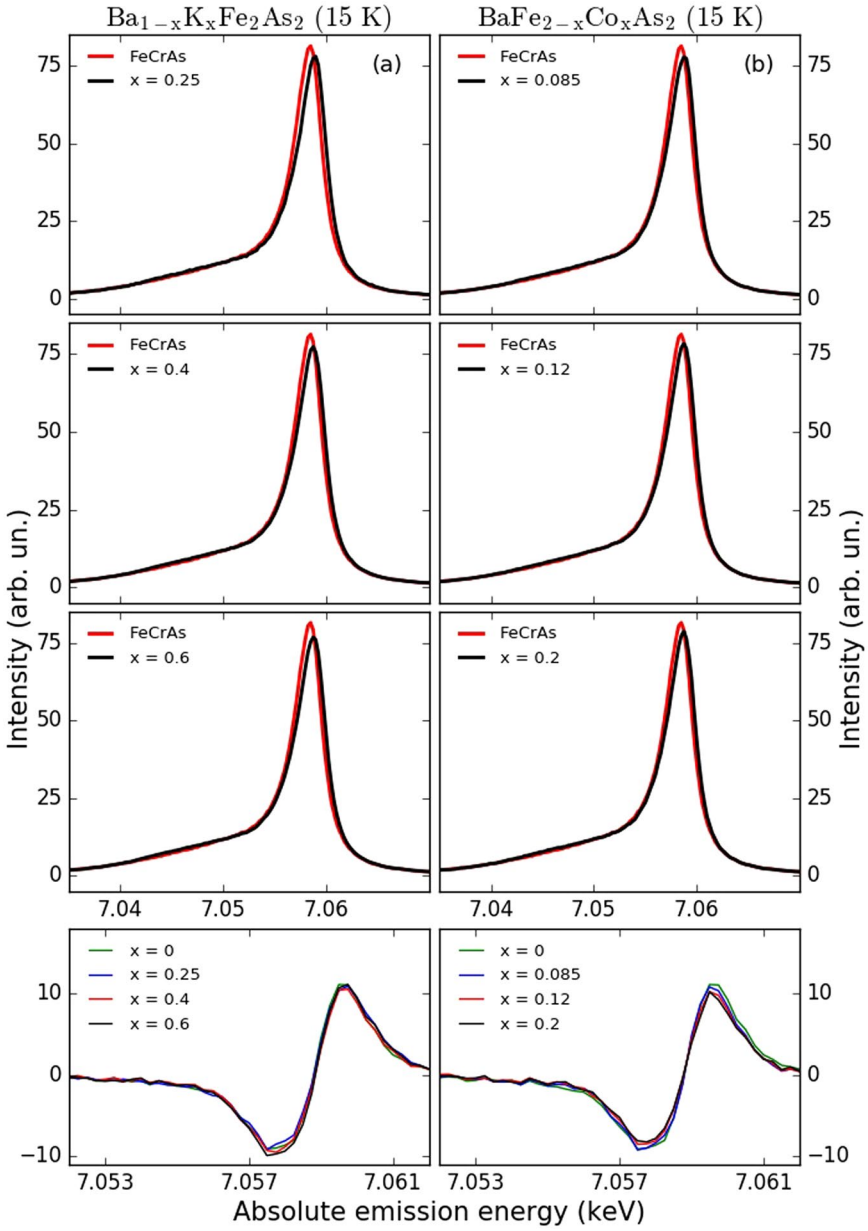

Figure 2. K_β XES for $Ba_{1-x}K_xFe_2As_2$ (**a**) with $x = 0.25$, 0.4, and 0.6 and $Ba_{1-x}K_xFe_2As_2$ (**b**) with $x = 0.085$, 0.12, and 0.2 at 15 K. The last row is indicating the relative difference spectra for $Ba_{1-x}K_xFe_2As_2$ and $Ba_{1-x}K_xFe_2As_2$.

additional step all the spectra to the centre of mass as described in ref. 60. We show the difference between the parent and reference compound as the shadowed part of Fig. 1(c). From the integration of this difference spectrum we obtain the IAD.

Having calibrated the instrumental response of IAD vs. μ_{bare}, we now quantify μ_{bare} in the doped compounds of $BaFe_2As_2$. In Fig. 2(a), we present the evolution of the XES for hole-doped $Ba_{1-x}K_xFe_2As_2$ samples with $x = 0.25$, 0.4, and 0.6 at 15 K. All spectra look very similar with almost no modification detectable. Consequently, the difference spectra shown in the bottom panels of Fig. 2(a) display little change of μ_{bare} with hole doping. Moving to the XES spectra of electron-doped $Ba_{1-x}K_xFe_2As_2$ ($x = 0.085$, 0.12, and 0.2) depicted in Fig. 2(b), we observe similar spectral features compared to hole-doped $BaFe_2As_2$. However, the IAD analysis shows here a decrease of μ_{bare} from $1.3 \pm 0.15\,\mu_B$ to $1.1 \pm 0.15\,\mu_B$ with Co doping.

We collected additional XES spectra at 300 K and plot them in Fig. 3(a) for $Ba_{1-x}K_xFe_2As_2$ (with $x = 0.25$, 0.4, and 0.6) and in Fig. 3(b) for $Ba_{1-x}K_xFe_2As_2$ (with $x = 0.085$, 0.12, and 0.2). The spectral shape is basically invariant with temperature, but the XES measurements at 300 K exhibit an *increase* of IAD and consequently an increase of μ_{bare} in all samples compared to the respective values at 15 K (Figs 3 and 4(a)).

These measurements are summarized in Fig. 4(a), where we plot the extracted μ_{bare} for all dopings at both temperatures. Additionally to μ_{bare}, we show in Fig. 4(a) on the right-hand side a relative scale of the IAD. In this scale, the IAD of the $BaFe_2As_2$ at 15 K is set to one and the relative change is displayed for all the other compounds. At

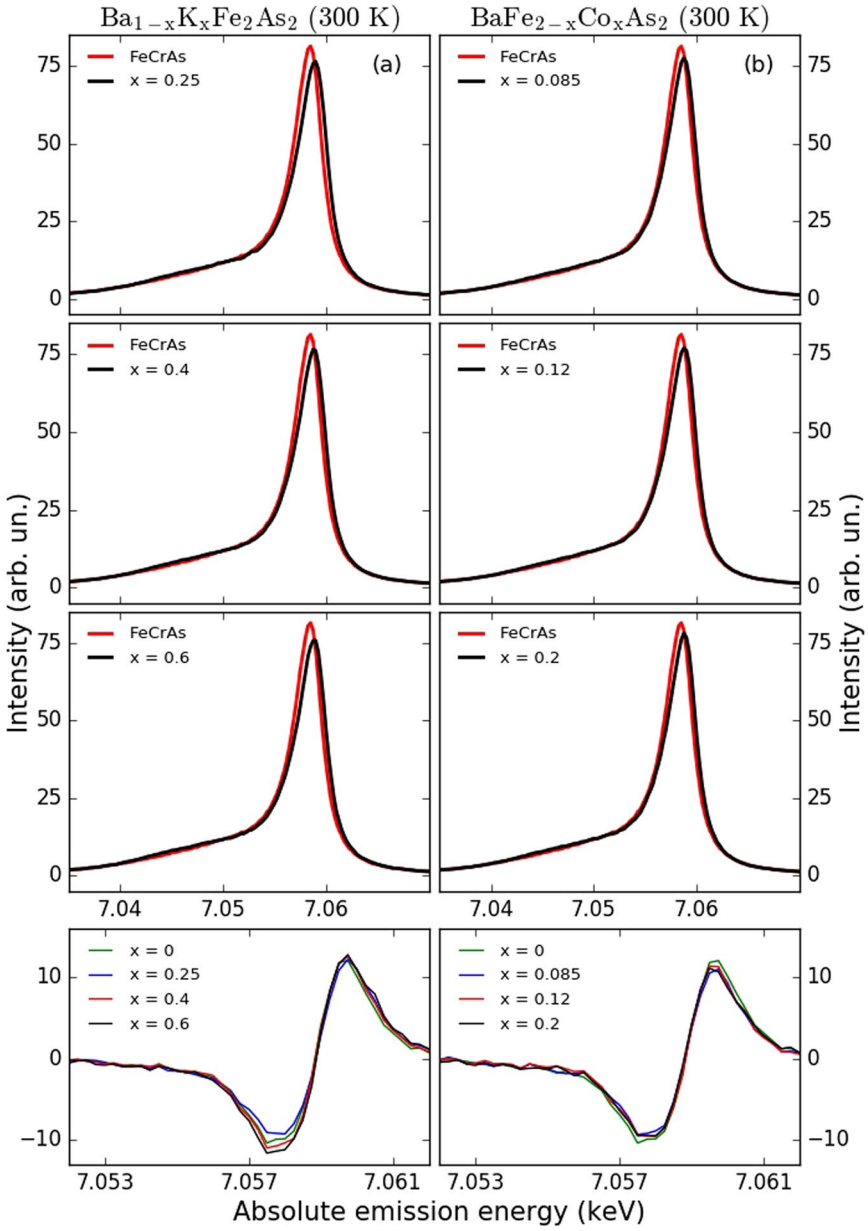

Figure 3. K_β XES at 300 K for $Ba_{1-x}K_xFe_2As_2$ (**a**) with $x = 0.25$, 0.4, and 0.6 and $Ba_{1-x}K_xFe_2As_2$ (**b**) with $x = 0.085$, 012, and 0.2 at 300 K. The last row is indicating the relative difference spectra for $Ba_{1-x}K_xFe_2As_2$ and $Ba_{1-x}K_xFe_2As_2$.

15 K, μ_{bare} remains approximately 1.3 μ_B in the hole-doped compounds and gradually decreases with doping in electron-doped compounds. This variation is remarkable considering the smaller number of electrons doped by Co-doping compared to the holes injected by K-doping as displayed in the bottom scale of Fig. 4(a). At 0.3 doped holes per Fe no change is observed, whereas doping of just 0.1 electrons per Fe induces a 15% decrease of μ_{bare}. All the samples display an increase of μ_{bare} with temperature, however this increase is surprisingly stronger on the hole-doped samples than in electron-doped ones as shown in Fig. 4(a).

We can partially explain our observations at low temperature by initially considering the fully itinerant limit, where the nesting strength and μ are connected, and can be quantified by the Lindhard function, which has been observed to evolve asymmetrically upon doping[61]. The nesting strength decreases linearly with the injection of electrons, but remains constant up to $x = 0.4$ for hole doping where it starts to decrease for even larger doping[61]. This could account for the decrease of μ_{bare} upon electron doping and partially explain the almost constant μ_{bare} for weak hole doping, but it clearly fails at higher hole doping concentrations.

Moreover, the lack of magnetic ordering, and the observation of a paramagnetic state with an increased μ_{bare} at 300 K, demonstrates that a Fermi surface nesting scenario completely fails to describe the evolution of μ at high temperature. Theoretical work suggested the importance of the Hund's coupling interaction and the need to combine local and itinerant physics to explain the magnetism of Fe pnictides[62–64]. The effect of doping has also

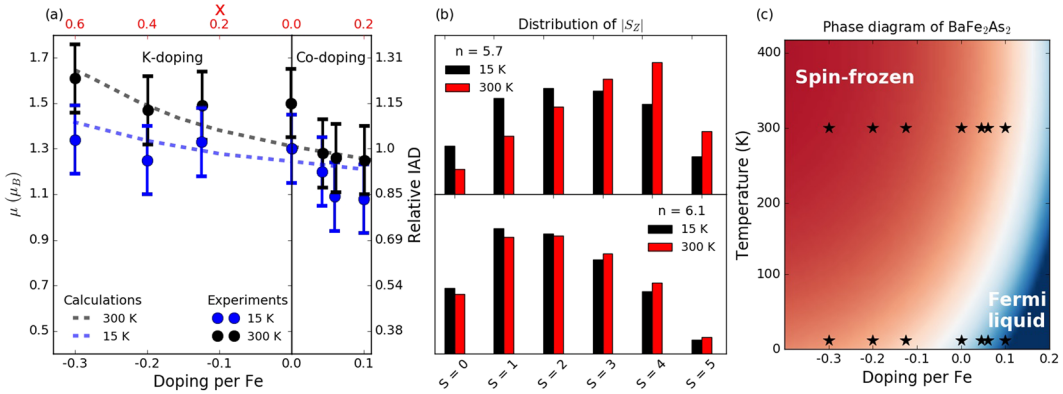

Figure 4. (**a**) Evolution of μ_{bare} and relative IAD for $Ba_{1-x}K_xFe_2As_2$ and $Ba_{1-x}K_xFe_2As_2$. The blue dots with error bars indicate measurements at 15 K, while the black dots with error bars represents μ_{bare} at 300 K. The dashed coloured lines are values for μ obtained from the DMFT calculations. The relative IAD scale is set to unity for $BaFe_2As_2$ at 15 K. (**b**) Distribution of $|S_z|$ values (in units of 1/2) in the thermal ensemble for $n = 5.7$ (top) and $n = 6.1$ (bottom) at 15 and 300 K. (**c**) Sketch of the theoretical phase diagram for $Ba_{1-x}K_xFe_2As_2$ and $Ba_{1-x}K_xFe_2As_2$ displaying the spin-frozen and Fermi liquid regimes and their evolution with doping and temperature.

been studied from both a theoretical and experimental standpoint, with the conclusion that doping does not only affect the carrier density and the chemical potential but also that the disorder induced by doping has to be taken into account, which can in principle account for the enhanced scattering rate upon doping[65,66].

Neutron scattering measurements of μ_{corr} show a good agreement with our findings on electron-doped samples[49], but a decrease is observed on hole-doped samples[48]. A difference in the evolution of magnetism upon hole doping has also been reported in INS and RIXS measurements of the spin excitations in $Ba_{1-x}K_xFe_2As_2$[12,48]. Both techniques detected consistently a decrease of the bandwidth of the spin excitations, but different results are observed in the intensity. INS detected a decrease of total intensity[48], whereas RIXS experiments showed a constancy in the intensity of the spin excitations[12]. This dichotomy may arise from the different region of the BZ zone probed by the two techniques[6], with INS having high sensitivity close to the antiferromagnetic ordering vector and RIXS measuring close to the Γ point. Generally this considerations make our data in agreement with RIXS experiments close to the Γ point.

When compared with our XES measurements, it is important to remember that μ_{bare} from XES, μ_{corr} probed by INS, and the spectral weight in RIXS have different correlation lengths. Our XES measurements probe the magnetic moment localized on a single Fe atom, whereas INS and RIXS can integrate along the momentum and energy domain obtaining μ_{corr} which is sensitive to to collective magnetic excitations. Thus in summary, they probe different aspects of the magnetism.

To aid the interpretation of the experimental measurements, we performed DMFT simulations of a five-orbital Hubbard model with a semi-circular density of states (DOS) of bandwidth 4 eV, which corresponds to the *d*-electron bandwidth of $Ba_{1-x}K_xFe_2As_2$ in the local density approximation[30]. The Coulomb interaction matrix was taken from ref. 30, but re-scaled in such a way that the SF crossover in the model with the simplified DOS occurs near *d*-electron filling $n_d = 6$ at temperature $T = 100$ K. (The fluctuating local moments at the border of the spin-frozen regime lead to a characteristic $\sqrt{\omega}$ frequency dependence of the self-energy[27], which can be used to identify this crossover regime.) We solved the DMFT equations using the hybridization-expansion approach[25], restricting the solution to paramagnetic metal states. The hybridization-expansion method gives direct access to the fluctuating Fe-3*d* states, and allows to calculate the instantaneous μ (here estimated as $\mu \approx \sqrt{\langle S_z \cdot S_z \rangle}$) in the relevant temperature and doping regime.

The calculations yield magnetic moments between 1.25 and 1.65 μ_B, in good agreement with the experimental results. We show the simulation results for temperatures $T = 15$ K and 300 K as dashed lines in Fig. 4(a). They display an increase of μ with hole doping and a decrease with electron doping in qualitatively good agreement with the experiments. The doping evolution can be ascribed to a change in the Fe-3 *d* filling, which affects the distribution of atomic states in the thermal ensemble. In particular, electron doping (hole doping) moves the system further away from (closer to) filling $n_d = 5$, which is needed to realize the maximum spin state in a localized picture. (In the experiments, the formal occupation is 3 $d^{6.1}$ and 3 $d^{5.7}$ at the highest dopings.) Most interestingly, our calculations also predict an increase of μ with increasing temperature, an effect which is particularly pronounced on the hole-doped side. Within the SF picture, this arises from a weaker Kondo screening of the local moments at high temperature. In this context, future experimental studies at intermediate temperatures might elucidate whether the magnetic moment increases continuously or if some discontinuous temperature development occurs. It is also instructive to look at the distribution of $|S_z|$ values in the thermal ensemble, which is plotted in panel (b) of Fig. 4. Especially on the hole-doped side, these histograms provide clear evidence for a weight shift towards high-spin states and reduced spin fluctuations at the higher temperature.

By correctly reproducing the experimentally observed stronger increase of μ_{bare} with temperature in hole-doped samples, our DMFT calculations confirm that this behaviour is a signature of a crossover into a

spin-frozen state. Figure 3(c) illustrates the consequences of the SF crossover on the nature of the metallic phase together with the respective position of the measured samples in the phase diagram (black stars). Hole doping shifts the Fe configuration towards half-filling, and the strong scattering from frozen moments wipes out the bandstructure and invalidates Fermi surface nesting arguments. On the other hand, electron doping leads the system away from the SF crossover region into a more conventional correlated metal regime, indicated by the blue region, where Fermi surface nesting arguments are applicable. This picture is consistent with recent optical measurements showing a non-Fermi liquid response for hole-doped $BaFe_2As_2$ and Fermi liquid behaviour for electron-doped $BaFe_2As_2$[67].

The difference in slopes observed between calculations and experiments in the electron-doped region and at low temperature may be explained as a consequence of competition between the Fermi surface nesting and the SF. As it is clear from Fig. 4(c), this is the only region of the explored phase diagram where there is a Fermi liquid phase. This suggests that Fermi surface nesting prevails over SF, so that the decrease of μ_{bare} arises mainly from a worsened nesting. This effect is not captured by DMFT calculations with a semi-circular DOS and is difficult to implement in such a theoretical framework. In this case a theoretical framework accounting for the detailed band structure of the system should be used instead of a simplified semi-circular DOS. The situation is opposite on the hole-doped side where Hund's-coupling and SF effects dominate nesting and μ_{bare} is more strongly affected by local physics. Despite the difficulty of our model to simulate the low temperature electron-doped region, it is remarkable that such a model based on few parameters can cover the evolution of the magnetic moment in a wide portion of the phase diagram as a function of both doping and temperature.

Another consideration concerns the *c* lattice parameter, which has been connected to the magnitude of the magnetic moment[6,68]. Specifically, the *c* lattice parameter has been observed to shrink in Co-doped samples and to increase in K-doped samples[69,70], implying an increase of hopping with Co doping leading to a Fermi liquid phase, and a decrease of hopping in the K-doped phase driving the system into a more correlated phase, i.e. the SF region. This connection between *c* lattice parameter and electronic correlations is in agreement with our interpretation of the evolution of μ_{bare} within the phase diagram, since the interaction effects are increased in hole-doped samples and decreased on the electron-doped side of the phase diagram (especially at low temperature).

Conclusions

In summary, we have measured μ_{bare} in hole- and electron-doped $BaFe_2As_2$ across the phase diagram. At 15 K, we found μ_{bare} to be weakly dependent on hole doping, but to clearly decrease upon electron doping, in agreement with a crossover between a SF phase and a correlated metal phase with well-defined Fermi surface. Our work demonstrates the importance of Hund's coupling in the description of Fe pnictides. The asymmetrical increase of μ_{bare} at 300 K results from a competition between electronic screening and Hund's-coupling induced local moment formation. The qualitative agreement between the doping and temperature dependence observed in both theory and experiment indicates that a SF occurs in hole-doped $BaFe_2As_2$, and that both Hund's-coupling and nesting effects are essential for understanding the unconventional metal state of Fe pnictides.

Methods

Single crystals of $BaFe_2As_2$, $Ba_{1-x}K_xFe_2As_2$, and $Ba_{1-x}K_xFe_2As_2$ have been grown by the flux method as described in refs 71, 72. We performed XES experiments at BL11XU of SPring-8, Hyogo, Japan. The incoming beam was monochromatized by a Si(111) double-crystal and a Si(400) secondary channel-cut crystal. The energy was calibrated by measuring X-ray absorption of an Fe foil and set to 7.140 keV with π polarization. We employed three spherical diced Ge(620) analyzers and a detector in Rowland geometry at ca 2 m distance. The total combined resolution was about 400 meV estimated from FWHM of the elastic line. We scanned the absolute emission energy between 7.02 keV and 7.08 keV and normalized the intensity by the incident flux monitored by an ionization chamber. We carried out measurements at both 15 and 300 K.

References

1. Kamihara, Y., Watanabe, T., Hirano, M. & Hosono, H. Iron-Based Layered Superconductor La[$O_{1-x}F_x$]FeAs (x=0.05–0.12) with T_c =26K. *Journal of the American Chemical Society* **130**, 3296–3297, doi:10.1021/ja800073m (2008).
2. Stewart, G. R. Superconductivity in iron compounds. *Reviews of Modern Physics* **83**, 1589–1652, doi:10.1103/RevModPhys.83.1589 (2011).
3. Johnston, D. C. The puzzle of high temperature superconductivity in layered iron pnictides and chalcogenides. *Advances in Physics* **59**, 803–1061, doi:10.1080/00018732.2010.513480 (2010).
4. Chubukov, A. V. Itinerant electron scenario for Fe-based superconductors http://xxx.tau.ac.il/abs/1507.03856 (2015).
5. *Iron-Based Superconductivity*, vol. 211 of *Springer Series in Materials Science* (Cham, doi:10.1007/978-3-319-11254-1 (2005).
6. Dai, P. Antiferromagnetic order and spin dynamics in iron-based superconductors. *Reviews of Modern Physics* **87**, 855–896, doi:10.1103/RevModPhys.87.855 (2015).
7. Dai, P., Hu, J. & Dagotto, E. Magnetism and its microscopic origin in iron-based high-temperature superconductors. *Nature Physics* **8**, 709–718, http://www.nature.com/nphys/journal/v8/n10/abs/nphys2438.html (2012).
8. Fawcett, E. Spin-density-wave antiferromagnetism in chromium. *Reviews of Modern Physics* **60**, 209–283, doi:10.1103/RevModPhys.60.209 (1988).
9. Richard, P., Sato, T., Nakayama, K., Takahashi, T. & Ding, H. Fe-based superconductors: an angle-resolved photoemission spectroscopy perspective. *Reports on Progress in Physics* **74**, 124512, http://stacks.iop.org/0034-4885/74/i=12/a=124512 (2011).
10. Mazin, I. I. Superconductivity gets an iron boost. *Nature* **464**, 183–186, http://www.nature.com/nature/journal/v464/n7286/abs/nature08914.html (2010).
11. Graser, S., Maier, T. A., Hirschfeld, P. J. & Scalapino, D. J. Near-degeneracy of several pairing channels in multiorbital models for the Fe pnictides. *New Journal of Physics* **11**, 025016, http://stacks.iop.org/1367-2630/11/i=2/a=025016 (2009).
12. Zhou, K.-J. *et al.* Persistent high-energy spin excitations in iron-pnictide superconductors. *Nature Communications* **4**, 1470, http://www.nature.com/ncomms/journal/v4/n2/full/ncomms2428.html (2013).
13. Pelliciari, J. *et al.* Intralayer doping effects on the high-energy magnetic correlations in NaFeAs. *Physical Review B* **93**, 134515, doi:10.1103/PhysRevB.93.134515 (2016).

14. Gretarsson, H. *et al*. Spin-State Transition in the Fe Pnictides. *Physical Review Letters* **110**, 047003, doi:10.1103/PhysRevLett.110.047003 (2013).
15. Gretarsson, H. *et al*. Revealing the dual nature of magnetism in iron pnictides and iron chalcogenides using x-ray emission spectroscopy. *Physical Review B* **84**, 100509, doi:10.1103/PhysRevB.84.100509 (2011).
16. Simonelli, L. *et al*. Coexistence of different electronic phases in the $K_{0.8}Fe_{1.6}Se_2$ superconductor: A bulk-sensitive hard x-ray spectroscopy study. *Physical Review B* **85**, 224510, doi:10.1103/PhysRevB.85.224510 (2012).
17. Vilmercati, P. *et al*. Itinerant electrons, local moments, and magnetic correlations in the pnictide superconductors $CeFeAsO_{1-x}F_x$ and $Sr(Fe_{1-x}Co_x)_2As_2$. *Physical Review B* **85**, 220503, doi:10.1103/PhysRevB.85.220503 (2012).
18. Bondino, F. *et al*. Electronic structure of $CeFeAsO_{1-x}F_x$ (x=0, 0.11, and 0.12). *Physical Review B* **82**, 014529, doi:10.1103/PhysRevB.82.014529 (2010).
19. Bondino, F. *et al*. Evidence for Strong Itinerant Spin Fluctuations in the Normal State of $CeFeAsO_{0.89}F_{0.11}$ Iron-Oxypnictide Superconductors. *Physical Review Letters* **101**, 267001, doi:10.1103/PhysRevLett.101.267001 (2008).
20. Mannella, N. The magnetic moment enigma in Fe-based high temperature superconductors. *Journal of Physics: Condensed Matter* **26**, 473202, http://stacks.iop.org/0953-8984/26/i=47/a=473202 (2014).
21. Yu, R. & Si, Q. Mott transition in multiorbital models for iron pnictides. *Physical Review B* **84**, 235115, doi:10.1103/PhysRevB.84.235115 (2011).
22. Si, Q. & Abrahams, E. Strong Correlations and Magnetic Frustration in the High T_c Iron Pnictides. *Physical Review Letters* **101**, 076401, doi:10.1103/PhysRevLett.101.076401 (2008).
23. Si, Q., Abrahams, E., Dai, J. & Zhu, J.-X. Correlation effects in the iron pnictides. *New Journal of Physics* **11**, 045001, http://stacks.iop.org/1367-2630/11/i=4/a=045001 (2009).
24. Georges, A., Kotliar, G., Krauth, W. & Rozenberg, M. J. Dynamical mean-field theory of strongly correlated fermion systems and the limit of infinite dimensions. *Rev. Mod. Phys.* **68**, 13–125, doi:10.1103/RevModPhys.68.13 (1996).
25. Werner, P., Comanac, A., de' Medici, L., Troyer, M. & Millis, A. J. Continuous-time solver for quantum impurity models. *Phys. Rev. Lett.* **97**, 076405, doi:10.1103/PhysRevLett.97.076405 (2006).
26. Werner, P. & Millis, A. J. Hybridization expansion impurity solver: General formulation and application to kondo lattice and two-orbital models. *Phys. Rev. B* **74**, 155107, doi:10.1103/PhysRevB.74.155107 (2006).
27. Werner, P., Gull, E., Troyer, M. & Millis, A. J. Spin Freezing Transition and Non-Fermi-Liquid Self-Energy in a Three-Orbital Model. *Physical Review Letters* **101**, 166405, doi:10.1103/PhysRevLett.101.166405 (2008).
28. Ishida, H. & Liebsch, A. Fermi-liquid, non-fermi-liquid, and mott phases in iron pnictides and cuprates. *Phys. Rev. B* **81**, 054513, doi:10.1103/PhysRevB.81.054513 (2010).
29. Haule, K. & Kotliar, G. Coherence-incoherence crossover in the normal state of iron oxypnictides and importance of hund's rule coupling. *New Journal of Physics* **11**, 025021, http://stacks.iop.org/1367-2630/11/i=2/a=025021 (2009).
30. Werner, P. *et al*. Satellites and large doping and temperature dependence of electronic properties in hole-doped $BaFe_2As_2$. *Nature Physics* **8**, 331–337, http://www.nature.com/nphys/journal/v8/n4/abs/nphys2250.html (2012).
31. Su, Y. *et al*. Antiferromagnetic ordering and structural phase transition in $BaFe_2As_2$ with Sn incorporated from the growth flux. *Physical Review B* **79**, 064504, doi:10.1103/PhysRevB.79.064504 (2009).
32. Kofu, M. *et al*. Neutron scattering investigation of the magnetic order in single crystalline $BaFe_2As_2$. *New Journal of Physics* **11**, 055001, http://stacks.iop.org/1367-2630/11/i=5/a=055001 (2009).
33. Kaneko, K. *et al*. Columnar magnetic structure coupled with orthorhombic distortion in the antiferromagnetic iron arsenide $SrFe_2As_2$. *Physical Review B* **78**, 212502, doi:10.1103/PhysRevB.78.212502 (2008).
34. Zhao, J. *et al*. Spin and lattice structures of single-crystalline $SrFe_2As_2$. *Physical Review B* **78**, 140504, doi:10.1103/PhysRevB.78.140504 (2008).
35. Aczel, A. A. *et al*. Muon-spin-relaxation studies of magnetic order and superfluid density in antiferromagnetic NdFeAsO, $BaFe_2As_2$, and superconducting $Ba_{1-x}K_xFe_2As_2$. *Physical Review B* **78**, 214503, doi:10.1103/PhysRevB.78.214503 (2008).
36. Kitagawa, K., Katayama, N., Ohgushi, K., Yoshida, M. & Takigawa, M. Commensurate Itinerant Antiferromagnetism in $BaFe_2As_2$: ^{75}As-NMR Studies on a Self-Flux Grown Single Crystal. *Journal of the Physical Society of Japan* **77**, 114709, doi:10.1143/JPSJ.77.114709 (2008).
37. Kitagawa, K., Katayama, N., Ohgushi, K. & Takigawa, M. Antiferromagnetism of $SrFe_2As_2$ Studied by Single-Crystal ^{75}As-NMR. *Journal of the Physical Society of Japan* **78**, 063706, doi:10.1143/JPSJ.78.063706 (2009).
38. Pratt, D. K. *et al*. Coexistence of Competing Antiferromagnetic and Superconducting Phases in the Underdoped $Ba(Fe_{0.953}Co_{0.047})_2As_2$ Compound Using X-ray and Neutron Scattering Techniques. *Physical Review Letters* **103**, 087001, doi:10.1103/PhysRevLett.103.087001 (2009).
39. Laplace, Y., Bobroff, J., Rullier-Albenque, F., Colson, D. & Forget, A. Atomic coexistence of superconductivity and incommensurate magnetic order in the pnictide $Ba(Fe_{1-x}Co_x)_2As_2$. *Physical Review B* **80**, 140501, doi:10.1103/PhysRevB.80.140501 (2009).
40. Bonville, P., Rullier-Albenque, F., Colson, D. & Forget, A. Incommensurate spin density wave in Co-doped $BaFe_2As_2$. *EPL* (*Europhysics Letters*) **89**, 67008, http://stacks.iop.org/0295-5075/89/i=6/a=67008 (2010).
41. Lumsden, M. D. & Christianson, A. D. Magnetism in Fe-based superconductors. *Journal of Physics: Condensed Matter* **22**, 203203, http://stacks.iop.org/0953-8984/22/i=20/a=203203 (2010).
42. Huang, Q. *et al*. Neutron-Diffraction Measurements of Magnetic Order and a Structural Transition in the Parent $BaFe_2As_2$ Compound of FeAs-Based High-Temperature Superconductors. *Physical Review Letters* **101**, 257003, doi:10.1103/PhysRevLett.101.257003 (2008).
43. Yamamoto, Y. *et al*. Origin of Pressure-induced Superconducting Phase in $K_xFe_{2-y}Se_2$ studied by Synchrotron X-ray Diffraction and Spectroscopy. *Scientific Reports* **6**, 30946, http://www.nature.com/srep/2016/160808/srep30946/full/srep30946.html (2016).
44. Hansmann, P. *et al*. Dichotomy between Large Local and Small Ordered Magnetic Moments in Iron-Based Superconductors. *Physical Review Letters* **104**, 197002, doi:10.1103/PhysRevLett.104.197002 (2010).
45. Simonelli, L. *et al*. Temperature dependence of iron local magnetic moment in phase-separated superconducting chalcogenide. *Physical Review B* **90**, 214516, doi:10.1103/PhysRevB.90.214516 (2014).
46. Lafuerza, S. *et al*. Evidences of Mott physics in iron pnictides from x-ray spectroscopy. *arXiv:1607.07417* [*cond-mat*], http://arxiv.org/abs/1607.07417.ArXiv: 1607.07417 (2016).
47. Zhao, K. *et al*. The collapsed tetragonal phase as a strongly covalent and fully nonmagnetic state: persistent magnetism with interlayer As-As bond formation in Rh-doped $Ca_{0.8}Sr_{0.2}Fe_2As_2$. *arXiv:1702.02398* [*cond-mat*], http://arxiv.org/abs/1702.02398. ArXiv: 1702.02398 (2017).
48. Wang, M. *et al*. Doping dependence of spin excitations and its correlations with high-temperature superconductivity in iron pnictides. *Nature Communications* **4**, http://www.nature.com/ncomms/2013/131204/ncomms3874/full/ncomms3874.html (2013).
49. Luo, H. *et al*. Electron doping evolution of the magnetic excitations in $BaFe_{2-x}Ni_xAs_2$. *Physical Review B* **88**, 144516, doi:10.1103/PhysRevB.88.144516 (2013).
50. Pelliciari, J. *et al*. Presence of magnetic excitations in SmFeAsO. *Applied Physics Letters* **109**, 122601, doi:10.1063/1.4962966 (2016).
51. Pelliciari, J. *et al*. Local and collective magnetism of $EuFe_2As_2$. *Physical Review B* **95**, 115152, doi:10.1103/PhysRevB.95.115152 (2017).
52. Yin, Z. P., Haule, K. & Kotliar, G. Fractional power-law behavior and its origin in iron-chalcogenide and ruthenate superconductors: Insights from first-principles calculations. *Phys. Rev. B* **86**, 195141, doi:10.1103/PhysRevB.86.195141 (2012).
53. Bergmann, U. & Glatzel, P. X-ray emission spectroscopy. *Photosynthesis Research* **102**, 255–266, doi:10.1007/s11120-009-9483-6 (2009).

54. Vankó, G. *et al*. Probing the 3d spin momentum with x-ray emission spectroscopy: The case of molecular spin transitions. *The Journal of Physical Chemistry B* **110**, 11647–11653, doi:10.1021/jp0615961 (2006).
55. Ortenzi, L. *et al*. Structural Origin of the Anomalous Temperature Dependence of the Local Magnetic Moments in the $CaFe_2As_2$ Family of Materials. *Physical Review Letters* **114**, 047001, doi:10.1103/PhysRevLett.114.047001 (2015).
56. Peng, G. *et al*. High-resolution manganese x-ray fluorescence spectroscopy. Oxidation-state and spin-state sensitivity. *Journal of the American Chemical Society* **116**, 2914–2920, doi:10.1021/ja00086a024 (1994).
57. Glatzel, P., Bergmann, U., de Groot, F. M. F. & Cramer, S. P. Influence of the core hole on K_β emission following photoionization or orbital electron capture: A comparison using MnO and $^{55}Fe_2O_3$. *Physical Review B* **64**, 045109, doi:10.1103/PhysRevB.64.045109 (2001).
58. Wu, W. *et al*. A novel non–Fermi-liquid state in the iron-pnictide FeCrAs. *EPL* (*Europhysics Letters*) **85**, 17009. http://stacks.iop.org/0295-5075/85/i=1/a=17009 (2009).
59. Ishida, S., Takiguchi, T., Fujii, S. & Asano, S. Magnetic properties and electronic structures of CrMZ (M=Fe, Co, Ni; Z=P, As). *Physica B: Condensed Matter* **217**, 87–96. http://www.sciencedirect.com/science/article/pii/0921452695005382 (1996).
60. Glatzel, P. & Bergmann, U. High resolution 1s core hole X-ray spectroscopy in 3d transition metal complexe–electronic and structural information. *Coordination Chemistry Reviews* **249**, 65–95, http://www.sciencedirect.com/science/article/pii/S0010854504001146 (2005).
61. Neupane, M. *et al*. Electron-hole asymmetry in the superconductivity of doped $BaFe_2As_2$ seen via the rigid chemical-potential shift in photoemission. *Physical Review B* **83**, 094522, doi:10.1103/PhysRevB.83.094522 (2011).
62. Tam, Y.-T., Yao, D.-X. & Ku, W. Itinerancy-Enhanced Quantum Fluctuation of Magnetic Moments in Iron-Based Superconductors. *Physical Review Letters* **115**, 117001, doi:10.1103/PhysRevLett.115.117001 (2015).
63. Yin, W.-G., Lee, C.-C. & Ku, W. Unified Picture for Magnetic Correlations in Iron-Based Superconductors. *Physical Review Letters* **105**, 107004, doi:10.1103/PhysRevLett.105.107004 (2010).
64. Lv, W., Krüger, F. & Phillips, P. Orbital ordering and unfrustrated (π,0) magnetism from degenerate double exchange in the iron pnictides. *Physical Review B* **82**, 045125, doi:10.1103/PhysRevB.82.045125 (2010).
65. Berlijn, T., Lin, C.-H., Garber, W. & Ku, W. Do Transition-Metal Substitutions Dope Carriers in Iron-Based Superconductors? *Physical Review Letters* **108**, 207003, doi:10.1103/PhysRevLett.108.207003 (2012).
66. Ye, Z. *et al*. Extraordinary Doping Effects on Quasiparticle Scattering and Bandwidth in Iron-Based Superconductors. *Physical Review X*. **4**, 031041, doi:10.1103/PhysRevX.4.031041 (2014).
67. Tytarenko, A., Huang, Y., de Visser, A., Johnston, S. & van Heumen, E. Direct observation of a Fermi liquid-like normal state in an iron-pnictide superconductor. *Scientific Reports* **5**, 12421, http://www.nature.com/articles/srep12421 (2015).
68. Zhang, C. *et al*. Effect of Pnictogen Height on Spin Waves in Iron Pnictides. *Physical Review Letters* **112**, 217202, doi:10.1103/PhysRevLett.112.217202 (2014).
69. Ni, N. *et al*. Effects of Co substitution on thermodynamic and transport properties and anisotropic H_{c2} in $Ba(Fe_{1-x}Co_x)_2As_2$ single crystals. *Physical Review B* **78**, 214515, doi:10.1103/PhysRevB.78.214515 (2008).
70. Avci, S. *et al*. Phase diagram of $Ba_{1-x}K_xFe_2As_2$. *Physical Review B* **85**, 184507, doi:10.1103/PhysRevB.85.184507 (2012).
71. Wang, X. F. *et al*. The peculiar physical properties and phase diagram of $Ba_{1-x}K_xFe_2As_2$ single crystals. *New Journal of Physics* **11**, 045003, http://stacks.iop.org/1367-2630/11/i=4/a=045003 (2009).
72. Zhang, C. *et al*. Neutron Scattering Studies of spin excitations in hole-doped $Ba_{0.67}K_{0.33}Fe_2As_2$ superconductor. *Scientific Reports* **1** http://www.nature.com/articles/srep00115 (2011).

Acknowledgements

J.P. and T.S. acknowledge financial support through the Dysenos AG by Kabelwerke Brugg AG Holding, Fachhochschule Nordwestschweiz, and the Paul Scherrer Institut. J. P. acknowledges financial support by the Swiss National Science Foundation Early Postdoc. Mobility fellowship Project No. P2FRP2_171824. The synchrotron radiation experiments were performed at BL11XU of SPring-8 with the approval of the Japan Synchrotron Radiation Research Institute (JASRI) (Proposals No. 2014A3502 and 2014B3502). We thank Y. Shimizu for the support during the experiments at SPring-8 and D. Casa for fabrication of the Ge(620) analyzers. The DMFT calculations were run on the Brutus cluster at ETH Zürich. This research was partly supported by the NCCR MARVEL, funded by the Swiss National Science Foundation. The works performed at IOP-CAS are supported by NSF & MOST through research projects. The single crystal growth work at Rice is supported by the US DOE, BES under Contract No. DE-SC0012311 (P.D.). Part of the materials work at Rice is also supported by the Robert A. Welch foundation Grant No. C-1893 (P.D.).

Author Contributions

T.S. and P.W. conceived the project, J.P., Y.H., K.I., H.D, and T.S. carried out the experiments, C.Z., P.D., G.F.C., L.X., X.W., and C.J. produced the samples, P.W. carried out the calculations, J.P., K.I., P.W., and T.S. wrote the manuscript with contributions from all the authors.

Additional Information

Competing Interests: The authors declare that they have no competing interests.

Publisher's note: Springer Nature remains neutral with regard to jurisdictional claims in published maps and institutional affiliations.